Available online at www.sciencedirect.com
ScienceDirect
Journal of the European Ceramic Society 30 (2010) 2991–2996
www.elsevier.com/locate/jeurceramsoc

Microstructure design by mechanical alloying

Thomaz Augusto Guisard Restivo, Sonia Regina Homem Mello-Castanho *

Nuclear and Energetic Research Institute, IPEN -Av. Lineu Prestes 2242, Cid. Universitária 05508000, São Paulo, SP, Brazil

Available online 29 March 2010

Abstract

Mixing and coprecipitation processes are, often, not enough in order to reach materials holding several functional components, like selective catalysts that must work simultaneously. Even though when a homogeneous and fine distribution of the constituents is obtained, the affinity between equal phase particles leads to coarsening during the consolidation (sintering) process, as well as on application, such as the material can loose high reactivity. The present work proposes a new consolidation route – sintering by activated surface (SAS) – that employs sacrificial metal layers to avoid coarsening and to increase the diffusion profiles during sintering, once high activity surfaces are exposed during the first sintering step. Regarding limited oxygen potential is established in the sintering atmosphere, the SAS effect is engaged when a specific projected powder microstructure obtained by mechanical alloying (MA) processing is provided. The MA is driven in such a way that yields cermet powders particles with lamellar pod-like like structures, as shown in the SEM image. This projected morphology comprises the ceramic round particles plated by thin metal layers or embedded on them.

Porous nickel–zirconia based cermets are studied with Cu and some selected refractory metal additives. The refractory metals are expected to repeal Cu, which remains in pure state at the cermet. By its turn, Cu addition is postulated to prevent coking when fuel-reforming reactions are involved at the application (e.g. in solid oxide fuel cells). Furthermore, Cu is desired since it promotes shrinkage and lower the sintering temperatures. The SAS process running under argon atmospheres with controlled oxygen partial pressure is found to further reduce the sintering temperature by 100–300 °C, for cermets final densities above 60%TD. The sintering behaviour depends on the chosen additive, being Ag, Cu and Mo the most effective ones. The resulted sintered parts attain a suitable density and phase dispersion for catalysis applications.

Keywords: Sintering by activated surface; Mechanical alloying; Cermet; SOFC

1. Introduction

Cermet materials are the key components to drive new applications in several engineering areas, where radically opposing properties can be combined, therefore allowing to build advanced devices and systems. One known example holds the cermets based on metallic nickel and yttria stabilized zirconia (Ni–YSZ) as the anode component of solid oxide fuel cells (SOFC).[1,2] A more recent application is the high temperature electrolysis (HTE) while external heat sources from a nuclear reactor can be employed with advantages.[3–5] In this sense, Cu–YSZ is also postulated.[6] The suitability of such cermets materials arises from their mixed electronic–ionic conduction paths, as well as the catalytic and biofuels reforming capability, giving rise to adopting of reusable energy cycles. Beside electrochemical applications, unique properties have been examined recently[7] for nanostructured cermets giving rise to develop superhard materials and electronic components. The percolation threshold plays an important role on such materials.[7,8]

The bibliographic search found two groups publishing works where the MA processing is used for this purpose: the first one deals with high temperature water electrolysis cathodes of Ni(Cu)–YSZ[9–11] and the second one with SOFC Ni–YSZ anode.[12] However, the last has reported the material preparation was not successful for Ni content over 20% in volume, which does not comply with the percolation requirements of the SOFC anodes. A further article investigates the preparation of the ceramic composite NiO–YSZ,[13] which must be reduced under hydrogen during 4 h to obtain the final cermet. Our articles have been demonstrated the MA can be successfully used to obtain directly porous cermets from metallic and ceramic starting powders at lower sintering temperatures.[14,15] The mechanical alloying route employed seeks a powder morphology where the metal and ceramics phases are intimated mixed, such as by embedding the ceramic particles under thin

* Corresponding author. Tel.: +55 11 3133 9200; fax: +55 11 3133 9376.
E-mail addresses: guisard@dglnet.com.br (T.A.G. Restivo), srmello@ipen.br (S.R.H. Mello-Castanho).

0955-2219/$ – see front matter © 2010 Elsevier Ltd. All rights reserved.
doi:10.1016/j.jeurceramsoc.2010.02.008

metallic films. This powder structure displays higher sinterability and allow the onset of the sintering by activated surface (SAS) consolidation process, directly leading to porous cermets with good properties. The SAS process is a new concept that states the exposing of high activity ceramic surfaces during the sintering heat cycle in order to trigger the densification at lower temperatures. Adherent metallic films, microforged by MA, are effectives on blocking the surface diffusion that reduces the powder activity at medium temperatures. The process is driven in such a way to fill the microsized and nanosized superficial defaults. Following up the sintering profile leads to the exposure of such surfaces by mechanisms like volatile oxides evaporation, limited coarsening, solving and reactive sintering.

The work studies YSZ-based cermets with Ni and Cu, Ag, Mo and W as additives, which can be postulated as SOFC anodes or HTE cathodes. The first selected additive, Cu, is expected to avoid carbon deposition[16,17] and increase the electrical conductivity. The second additive is chosen into the refractory metals group (Mo, W, Nb, Ta) and Ag accordingly to their ability on triggering the SAS process, besides low Cu alloy solubility and similar hydride formation enthalpy as Ni.[18] The approach is based on the thermodynamics of immiscible systems on considering the repulsive interaction between Cu and C,[19,20] opposing to C deposition at the electrode surface. By the other side, Cu and Ni form easily an alloy at high temperatures, decreasing the own Ni activity and harming the C repulsion effect. Therefore, the second metallic additive is admixed in order to repulse itself the Cu atoms at a precipitated state.

2. Experimental

The starting powders were a cubic stabilized zirconia with 8 mol% yttria (YSZ, Tosoh Co.), BET 13 m^2/g, $d(50) = 0.3$ μm and 2 types of metallic Ni: $d(50) = 27$ μm atomized, 99.7 wt% pure and a high purity Ni powder (99.9 wt%, Aldrich) $d(50) = 3$ μm, while Cu powder had the same characteristics. Other additives with average particle sizes of 5 μm were employed: W, Mo, Nb, Ta and Ag. In an experimental setup Ni and Mo powders were previously annealed at 750 and 1100 °C, respectively. The high energy milling (MA) was carried out at shaker mills rated at 19 Hz with VC131 steel vials and AISI 52100 spheres ϕ5 mm as milling media with balls to powder ratio of 10:1. The loaded vials were sealed under vacuum and submitted to the milling process during 3–8 h. The resulted contamination is limited to low content of Fe and Cr (0.3 wt%). All prepared compositions were set to 40 vol.% metal content and 60 vol.% YSZ, where the additives summed 20 vol.%:12 vol.% Cu and 8 vol.% of a third metal, if present. The MA processing sequence employed searches a powder microstructure where Cu particles remain insulated, interposed by the refractory metal layers. The whole lamellar assembling is disposed in such a manner to coat the round thin YSZ particles on a pod-like morphology type (Fig. 1). The YSZ particles can either be embedded over the lamellae. The powder samples were pressed uniaxially under 150 MPa load into 7 and 10 mm diameter dies.

The SAS process was carried out at a tubular furnace under argon flow (150 mL/min) with 2, 5 and 10 vol.% water vapour by saturating the inlet flow line in a distilled water flask at a controlled temperature. All the experiments were performed at a 10 °C/min heating rate and 1-h isotherm at the maximum temperature. The oxygen partial pressure was estimated through thermodynamic calculation related to water vapour decomposition at each sintering temperature. The powders and pellets were analysed at scanning and transmission electron microscopes, as well as by X-ray diffraction.

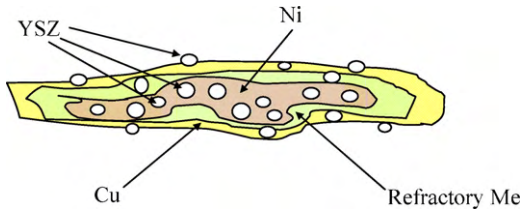

Fig. 1. Sequential MA processing target microstructure: lamellar pod-like.

The sintering kinetics was investigated by the stepwise isothermal dilatometry (SID) method at a Setaram TMA/dilatometer (Labsys TMA 1400 °C) under small load (2 g) to avoid any influence from the probe contact pressure on the retraction. The SID analysis is based on the quasi-isothermal dilatometry,[21–24] where an equation type like $dy/dt = K(T).f(y)$ is searched, being y the measured dimension as a function of time. In this particular method, several 15-min isotherms are programmed at 50 °C intervals during the heating at 10 °C/min along the length of the relevant temperature range. The model develops from the basic shrinkage equation[25–27]:

$$\frac{\Delta L}{L_o} = y = [K(T).t]^n \tag{1}$$

where $K(T)$ is a constant which is analogous to the reaction rate and n is a parameter related to diffusion mechanisms, also equivalent to reaction order. Assuming the sintering process is isotropic, the normalized volumetric shrinkage can be written as $Y = (V_o - V_t)/(V_o - V_f) = ({L_o}^3 - {L_t}^3)/({L_o}^3 - {L_f}^3)$, where the indexes o, t and f indicate the initial, at the time t and final dimensions, respectively. By replacing the relative linear retraction at Eq. (1) by the relative volumetric retraction $Y/(1-Y) = (V_o - V_t)/(V_t - V_f)$, followed by differentiation on time, one can obtain the normalized retraction equation[28]:

$$\frac{dY}{dt} = nK(T)Y(1-Y)\left[\frac{(1-Y)}{Y}\right]^{1/n} \tag{2}$$

At each isotherm, the plot $\ln\{(dY/dt)[1/Y(1-Y)]\}$ versus $\ln[(1-Y)/Y]$ yields a straight line whereby the n and $K(T)$ parameters can be determined as the slope and intercept. The reaction rate obeys the Arrhenius relationship:

$$K(T) = A\ \exp\left(-\frac{Q}{RT}\right) \Rightarrow \ln[K(T)] = \ln\ A - \frac{Q}{RT} \tag{3}$$

Finally, the process apparent activation energy Q can be determined from the $n[K(T)] \times 1/T$ plot.

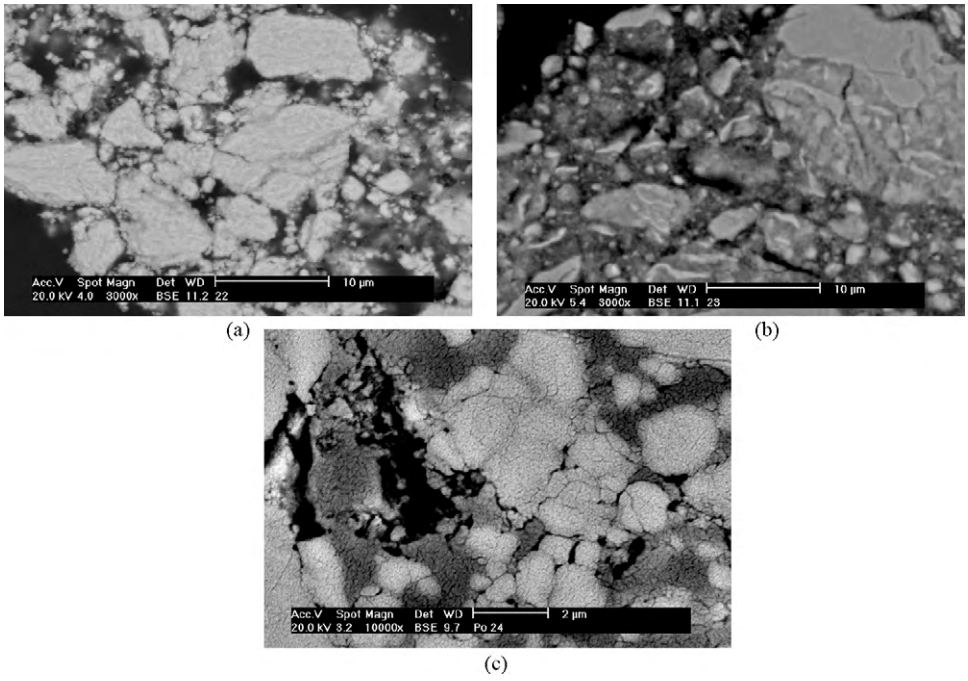

Fig. 2. MA processed SEM/BSE images: (a) Ni–YSZ 4 h MA, (b) Cu–Ni (27 μm)–YSZ 3 h MA and (c) Cu–Ni(3 μm)–YSZ 3 h MA.

3. Results and discussion

The Ni(Cu)–YSZ MA processed powders assume a lamellar morphology with highly dispersed constituents, as shown in Fig. 2. The metallic rich phases show brighter contrast under back-scattered SEM images. However, the phases are dispersed at a nanometric level, once both bright and dark fields contain Ni (Cu) and YSZ, as found by punctual EDS analyses. The lamellae are less elongated for the Cu–Ni–YSZ powder prepared from 3 μm Ni fine powder. Pod-like like morphology evidences are best seen through resin impregnated samples in SEM or higher magnifications of TEM microscope (Fig. 3). Some nodular particles are found between the lamellae or embedded on them.

A compilation of sintered pellet microstructures at 1300 °C in argon atmosphere is shown in Fig. 4. The appearance of liquid phase sintering is more evident at Cu-bearing pellets whose are also denser. Cu promotes the connection among the gray ceramic phase and the reduction of the porosity. One can note the progressive refining when Cu is added, as well as when employing the lower particle size Ni starting powder (3 μm). Some white nodules observed are YSZ remaining particles, immersed in the metal.

The sintering kinetics results accordingly the SID method (Eq. (2)) demonstrates that Cu addition promotes the densification. The apparent activation energies for the sintering process at high temperature are rather smaller when Cu replaces 30 vol.% of Ni (Fig. 5). The Cu-bearing material tends to shrink with low

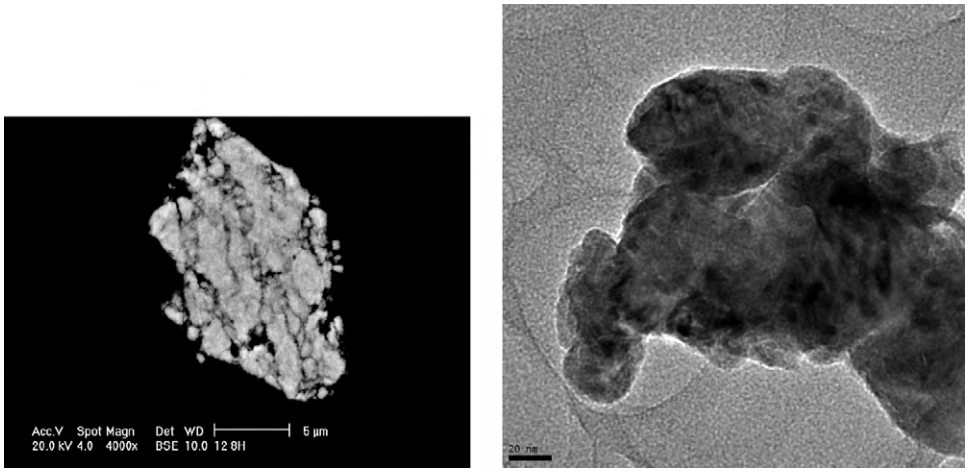

Fig. 3. Ni–YSZ powder – MA 8 h – SEM image (upper); Cu–Ni–YSZ powder – MA 3 h – TEM image (right).

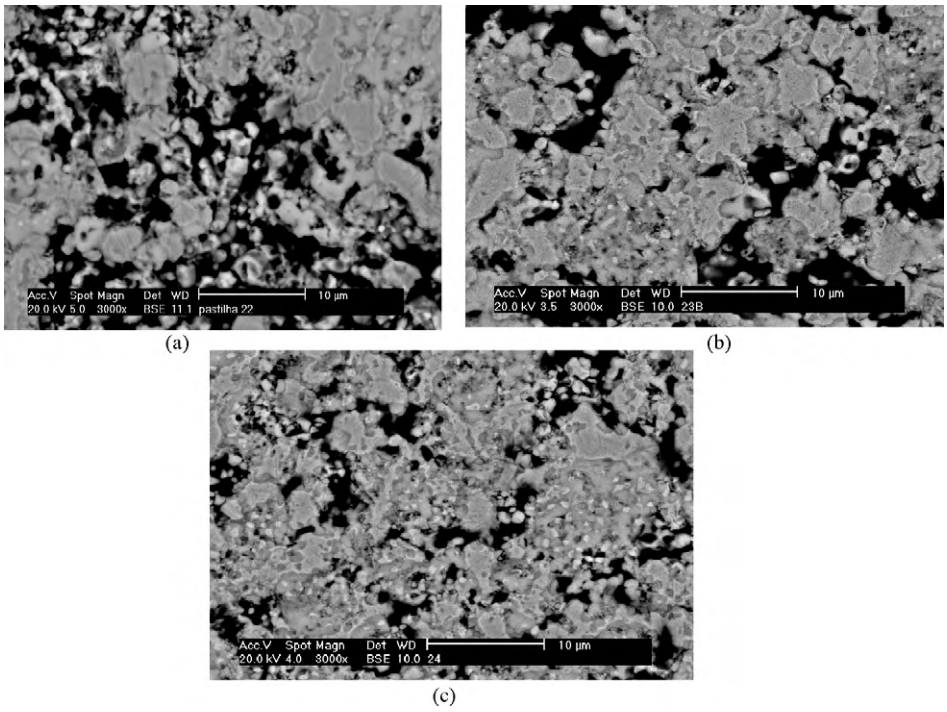

Fig. 4. Sintered pellets SEM/BSE images, 1300 °C in argon: (a) Ni–YSZ; (b) Cu–Ni(27 μm)–YSZ; (c) Cu–Ni(3 μm)–YSZ.

activation energy either at low temperatures, where a straight line can be defined on Arrhenius plot. Previous results[14,15] suggest the cermet sinters at low temperatures by metallic constituents with low activation energy. At higher temperatures (>750 °C) there is a mechanism change and the sintering of ceramic phase becomes the rate-controlling step with high activation energy. Cu addition promotes sintering at both temperature ranges, in agreement with the observed microstructures.

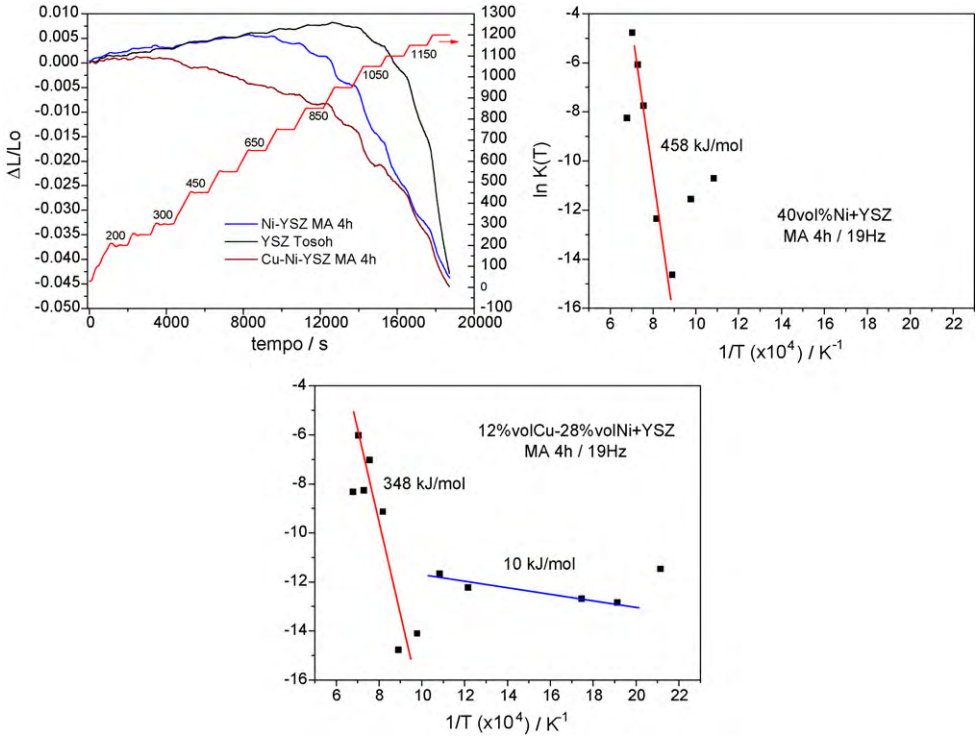

Fig. 5. Arrhenius plots derived from sintering kinetics data by SID method; upper: measured shrinkage.

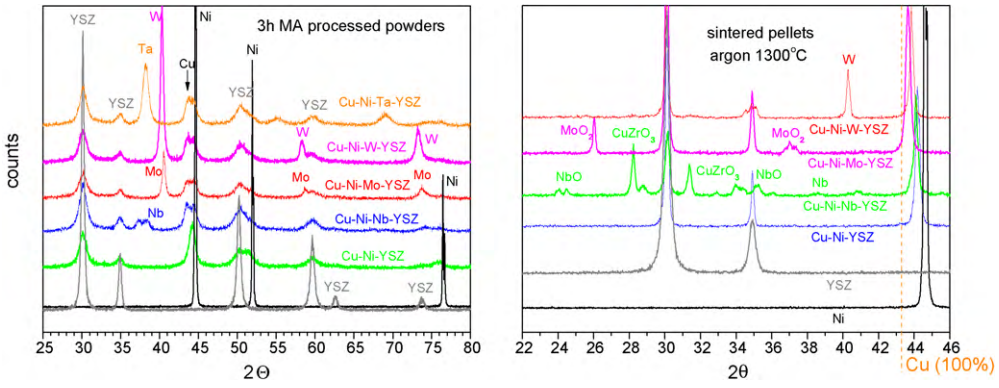

Fig. 6. Cu–Ni–YSZ powders (left) and sintered pellets X-ray diffractograms with refractory metals additives.

3.1. Multi-metallic electrodes

Accordingly to powder X-ray diffraction previous results,[14,15] Ni forms alloy with Cu early at the high energy milling step. Further replacing metals, selected among the refractory group, avoid the premature Ni–Cu alloy formation. Fig. 6 compiles the powder and 1300 °C sintered pellets diffractograms for Cu–Ni–YSZ samples with 8 vol.% of W, Nb, Mo and Ta. The material without such refractory additives does not show Cu reflection peak ($2\theta = 43{,}295°$ (100%), JCPDF 04-0836), but rather a Ni peak shifting to smaller angles, meaning the alloy Cu–Ni is readily formed during the MA processing. Nevertheless the materials doped with refractory metals show clearly the Cu (1 1 0) peaks. This fact is explained by strong repulsive interactions between Cu and these metals, which is verified by the respective phase diagrams, displaying nil solubility and no alloy formation. Along the MA processing the interphase distances are shortened down to a sub-micrometer level and the Ni and Cu phases can be interposed by the refractory metal layers, causing Cu repulsion or acting as diffusion barriers. However, the situation is not conserved after sintering at 1300 °C, when new phases are formed.

3.2. Sintering by activated surface – SAS

Fig. 7 shows the 1200 °C sintered density values and mass loss as a function of temperature and oxygen partial pressure for the metallic phases added to YSZ. One can note the Ni–YSZ, Cu–Ni(27 μm)–YSZ and the sample doped with Mo reach higher densities under 5 vol.% of H_2O_v, corresponding to $PO_2 = 582 \times 10^{-6}$ atm, whose densities are similar to the same samples sintered at 1300 °C in pure argon. By its turn, the Cu–Ni(3 μm)–YSZ material shows a less effective behaviour under SAS conditions compared to 1300 °C in argon, becoming more dense in the last. The cermets doped with W densify strongly at pure argon atmosphere since their respective oxide layers formed with higher oxygen potentials are more stable and work as sintering barriers. Actually the SAS process is engaged when any volatile oxide is formed, like MoO_3 and NiO_x, at oxygen potentials being of the same magnitude compared to the own oxide formation ($\sim 10^{-6}$ atm). The sample doped with Ag (Fig. 8) shows high density by SAS process even at 1100 °C, due to the lower melting point of Ag metal among the additives studied. However, at higher temperatures, the Ag evaporation is excessive at a point that the densification is constrained. The Ni–YSZ-based cermets consolidation can be performed by the SAS process, which can lower the usual sintering temperature (1300–1450 °C) by more than 300 °C. Most part of the studied cermet compositions reach suitable density for SOFC and the electrode applications (60–70%TD) early at 1000 °C/1 h under SAS mode.

Fig. 9 shows a compilation with emphasis on Mo bearing cermets while the increasing PO_2 is obtained for 2, 5 and 10 vol.% water vapour. The Ni and Mo annealed powders at 750 and 1100 °C, respectively, prior to the milling process to confer some ductility, have been found important to attain higher density at small PO_2. These findings are based on the easiness on obtaining the pod-like morphology.

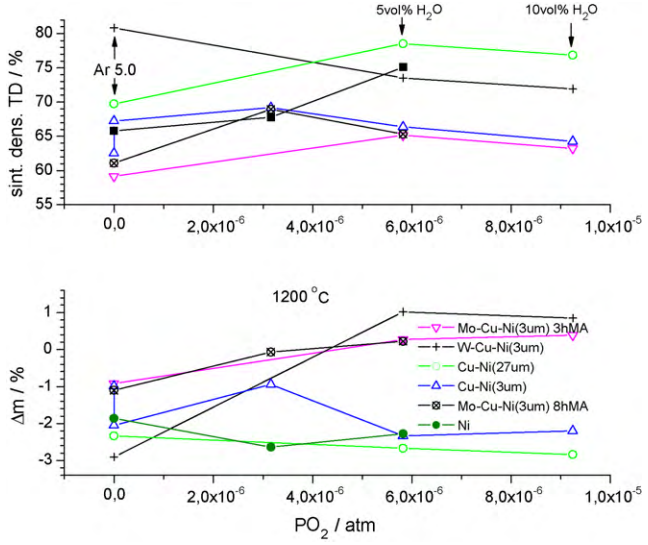

Fig. 7. Densification and mass loss results for cermets submitted to sintering by activated surface – SAS process.

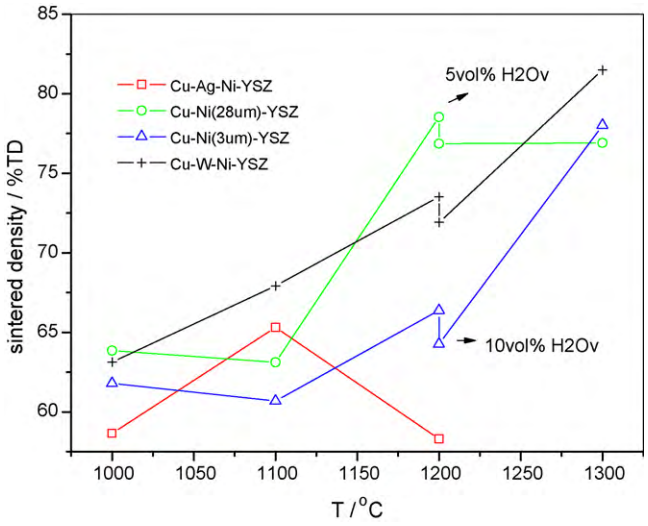

Fig. 8. SAS process as a function of temperature.

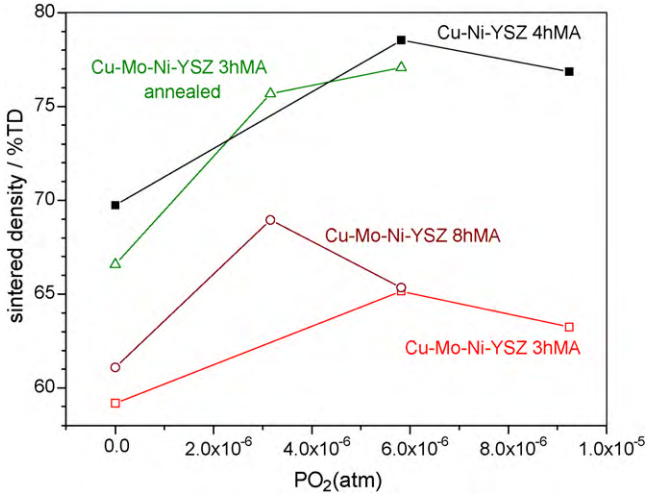

Fig. 9. Detailed study of Mo bearing materials sintered at 1200 °C at different oxygen potentials; Mo bearing cermets obtained with 3 and 8 h of MA and employing Ni and Mo annealed powders at 750 and 1100 °C, respectively.

4. Conclusions

The allied process MA–SAS leads to suitable cermet powders and sintered parts with good properties for applications as SOFC and HTE electrodes. The sintering kinetics study indicates the Cu addition promote the densification and refines the final microstructure. The refractory metals addition is efficient in order to avoid the premature Cu–Ni alloy formation during high energy milling processing. The additives Ag, W, Cu, Mo promotes the sintering at lower temperatures and oxygen potentials. The sintering by activated surface (SAS) process is effective to increase the density at lower temperatures, especially if some component yields a volatile oxide under the imposed controlled oxygen potential. The pod-like morphology is imperative to drive such sintering process. The combined MA–SAS process is promised as a cermet preparation method for cermet applications with superior performance.

The authors acknowledge the research councils FAPESP, CNPq, FINEP and CAPES for the financial support.

References

1. Atkinson A, Barnett S, Gorte RJ, Irvine JTS. *Nature Materials* 2004;**3**(1):17–27.
2. Minh NQ. *Journal of the American Ceramic Society* 1993;**76**(3):563–88.
3. Holladay JD, Hu JD, King L, Wang Y. *Catalysis Today* 2009;**139**:244–60.
4. Hino R, Haga K, Hideki A, Kenji S. *Nuclear Engineering and Design* 2004;**233**:363–75.
5. Hong HS, Chae U-S, Choo S-T. *Journal of Alloys and Compounds* 2008;**449**:331–4.
6. Kang K-H, S.L., Kim J-M, Hong HS, Yun Y, Woo S-K. *Journal of Alloys and Compounds* 2008;**448**:363–7.
7. Moya JS, Lopez-Steban S, Pecharromán C. *Progress in Materials Science* 2007;**52**:1017–90.
8. Lopez-Steban S, Bartolomé JF, Pecharromán C, Mello Castanho SRH, Moya JS. *Materials Research* 2001;**4**(3):217–22.
9. Hong HS, Chae U, Choo S, Lee KS. *Journal of Power Sources* 2005;**149**:84–9.
10. Hong HS, Chae U, Choo S. *Materials Science Forum* 2005;**486–487**:662–5.
11. Lee S, Kang K, Kim J, Hong HS, Yun Y, Wu S. *Journal of Alloys and Compounds* 2008;**448**:363–7, doi:10.1016/j.jallcom.2007.08.022.
12. Wilkenhoener R. *Journal of Materials Science* 1999;**34**:257–65.
13. Cho HJ, Choi GM. *Journal of Power Sources* 2008;**176**:96–101.
14. Restivo TAG, Mello-Castanho SRH. *Journal of Power Sources* 2008;**185**:1262–6.
15. Restivo TAG, Mello-Castanho SRH. *Materials Science Forum* 2008;**591–593**:514–20.
16. Gross MD, Vohs JM, Gorte RJ. *Electrochmica Acta* 2007;**52**(5):1951–7.
17. Sun C, Stimming U. *Journal of Power Sources* 2007, doi:10.1016/j.jpowsour.2007.06.086.
18. Fukai Y. *The metal–hydrogen system*. Springer; 1993.
19. Restivo TAG, Tese de Doutorado, Escola Politécnica USP; 2003. 106 p.
20. Restivo TAG, Capocchi JDT. *Journal of Nuclear Materials* 2004;**334**:189–94.
21. Sorensen OT. *Journal of Thermal Analysis* 1992;**38**:213–28.
22. Husum PL, Sorensen OT. *Thermochimica Acta* 1987;**114**:131–8.
23. Restivo TAG, Pagano Jr L. Sintering studies on the UO2.Gd2O3 system using SID method. In: *Conference on characterization and quality control of nuclear fuels 2002*. 2003.
24. Restivo TAG, Pagano Jr L. Effect of additives on the sintering kinetics of the UO2. Gd2O3 system. In: *Technical committee meeting on improved fuel pellet materials and designs, October 20–24*. 2003, paper 2.5.
25. El Sayed Ali M., Sorensen OT. Riso-R-518;1985. 12 p.
26. Wang H, Liu X, Chen FG, Meng, Sorensen OT. *Journal of the American Ceramic Society* 1998;**81**(3):781–4.
27. Bellon O. *Dilatometric sintering studies of zirconia toughened ceramics*. Centre for Advanced Technical Ceramics. Ecole Nationale Superieure de Ceramiques Industrielles. Risoe National Laboratory; 1991, 25 p.
28. Yan R, Chu F, Ma Q, Liu X, Meng G. *Materials Letters* 2006;**60**:3605–9.